공학석사 학위논문

Dual Echo Trajectory for Novel Fast Acquisition

Comparison to Partial Fourier Acquisition

2017 년 2 월

서울대학교 대학원

전기정보공학과

김 지 훈

Dual Echo Trajectory for Novel Fast Acquisition

Comparison to Partial Fourier Acquisition

지도 교수 이 종 호

이 논문을 공학석사 학위논문으로 제출함

2016 년 11 월

서울대학교 대학원

전기정보공학과

김 지 훈

김지훈의 공학석사 학위논문을 인준함

2016 년 12 월

위 원 장 김 성 준 (인)

부위원장 이 종 호 (인)

위 원 오 세 홍 (인)

Content

List of Figures

Abstract

Dual Echo Trajectory for Novel Fast Acquisition

Comparison to Partial Fourier Acquisition

Jee Hun Kim
Dept. of Electrical and Computer Engineering
The Graduate School
Seoul National University

The use of magnetic resonance imaging (MRI) allowed the exploration of human brain without exposure to dangerous radiation. With the aid of this wonderful technique, researchers and clinicians have pushed forward the frontiers of knowledge. Among the various methods used in MRI, the spin echo imaging produces valuable T1, T2 weighted images while reducing the image loss caused by the B_0 field inhomogeneity. This dissertation introduces a novel method to accelerate the acquisition of the spin echo image. The method consists of a new pulse sequence and corresponding correction and reconstruction method.

Keywords : magnetic resonance imaging, pulse sequence, spin echo imaging, fast acquisition
Student Number : 2015-20908

Chapter 1.Introduction

1.1 MRI Basics

In this chapter, a brief overview of basic theory of magnetic resonance imaging (MRI) will be introduced. The overview will focus on the basic theory of MRI and spin echo imaging. For more information, textbooks written by Nishimura [1] and Bernstein et al. [2] are rich with detailed explanations.

1.1.1 Signal Source

Atomic nuclei consist of protons and neutrons. These components are fermionic particles of spin 1/2. Spin is another word for angular momentum in quantum physics, and just like in classical mechanics where electrically charged objects with angular momentum can be considered as magnetic moment, spin $\boldsymbol{S}$ can be related to magnetic moment $\boldsymbol{\mu}$ by gyromagnetic ratio γ according to the following equation.

$$\boldsymbol{\mu} = \gamma \boldsymbol{S}$$

While for some of the atomic nuclei the total spin components sum up to zero, some nuclei such as hydrogen (^{1}H), carbon (^{13}C), oxygen (^{17}O), fluorescence (^{19}F), and phosphorus (^{31}P) have residual spin. As explained by the previous equation, the extra spin

makes these nuclei to act as magnetic moments. Particularly, ^{1}H, which is most abundant in the human body, is the partial signal source of MRI.

1.1.2 Nuclear Magnetic Resonance

The previously explained signal sources, atomic nuclei acting as magnetic moment, can be measured by a phenomenon called nuclear magnetic resonance (NMR) which was experimentally discovered in 1946 by Purcell [3] and Bloch [4]. In NMR, when external magnetic field is applied to nuclei with an odd number of neutrons or protons, they absorb and release energy in the form of electromagnetic wave. This electromagnetic wave has a particular resonance frequency called the Larmor frequency. This resonance frequency is defined by the following equation

$$\boldsymbol{\omega} = \gamma \boldsymbol{B}$$

where $\boldsymbol{\omega}$ is the resonance frequency, $\boldsymbol{B}$ is the applied external magnetic field, and γ is the gyromagnetic ratio. The gyromagnetic ratio of the hydrogen atom is 267.513×10^{6} rad/s/Tesla (or 42.58 MHz/Tesla).

The whole phenomenon starts from nuclear spin, which is a quantum mechanical concept. However, a classical vector model can successfully explain the complex nature in a much easier way illustrated. In this model, the whole process of NMR is described by two steps, polarization and excitation.

The polarization step is illustrated in Figure 1.1. A nuclear with a magnetic moment, in other word magnetization, is modeled as a vector with the particular resonance frequency. First, with no external magnetic field applied, these vectors point random directions as in Figure 1.1.a. Since they point random directions, the net magnetization, which is the sum of all vectors, is zero. When external magnetic field (B_0 field) is applied, they align to the direction of this field as in Figure 1.1.b. The net magnetization is now non-zero and points the direction of the external magnetic field. The net magnetization is influenced by several factors such as the gyromagnetic ratio of the imaging nuclei, the strength of B_0 field, spin density, and temperature. The net magnetization is important because it is directly related to the signal measured by NMR.

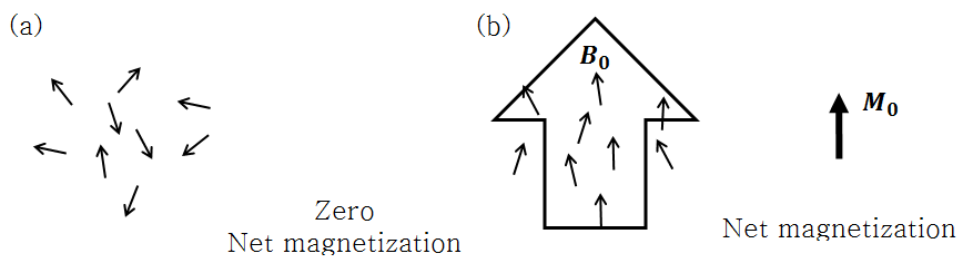

Figure 1.1 The polarization step of classical vector model to explain the behavior of nuclear spin. **a.** Without external field, vectors indicating each magnetic moment of nuclear spin point random directions, resulting in zero net magnetization. **b.** With external magnetic field ($\boldsymbol{B_0}$ field), spins are aligned to the direction of this field, forming the net magnetization in the same direction.

The next step, excitation step, is shown in Figure 1.2. The net

magnetization produced by previous polarization step points the direction of B_0 field, which is z−axis as shown in Figure 1.2.a. In MRI, the z component of magnetization is called longitudinal magnetization, and xy component of magnetization is called transverse magnetization. Excitation of this magnetization is achieved when an electromagnetic wave (EM wave) with the resonance frequency, Larmor frequency, is applied. This EM wave is called B_1 field, or radiofrequency pulse (RF pulse) since the Larmor frequency is in the radiofrequency range in clinical use (63.9 MHz for 1.5 Tesla B_0 field and 128 MHz for 3 Tesla B_0 field). Since the magnetization received energy, the direction deviates from the original direction as in Figure 1.2.b. In another word, the longitudinal magnetization gets smaller, and transverse magnetization grows. The angle between the equilibrium state and excited state is called the flip angle. The shape, magnitude, and duration of RF pulse determine this quantity. Throughout the process, the transverse magnetization precesses in Larmor frequency. When B_1 field is cut, the magnetization loses energy, recovering the original magnetization. Figure 1.2.c illustrates this process. The precessing transverse magnetization also produces EM wave in Larmor frequency, and an external receiver detects this by electromagnetic induction explained by the Faraday's law.

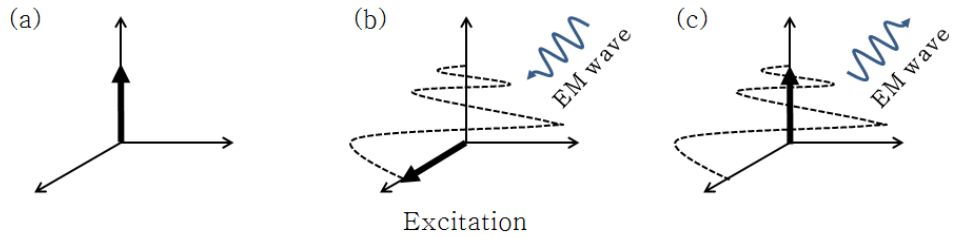

Figure 1.2 The excitation steps of NMR. **a.** Right after polarization, the whole magnetization lies on the z−axis, which is the direction of $\boldsymbol{B_0}$ field. **b.** When EM wave, or RF pulse, with Larmor frequency, is applied, the magnetization gains energy, and magnetization deviates from the original direction. **c.** After the excitation is turned off, the magnetization recovers the original state, and along the process, EM wave with Larmor frequency is emitted.

1.1.3 Bloch Equation

The Bloch equation, which was found by Bloch in 1946 [4], formulates the NMR phenomenon mathematically. The equation is as follows

$$\frac{d\boldsymbol{M}}{dt} = \gamma \boldsymbol{M} \times \boldsymbol{B} - \frac{M_x \hat{x} + M_y \hat{y}}{T_2} + \frac{M_0 - M_z}{T_1} \hat{z}$$

$\boldsymbol{M}$ denotes the magnetization, where M_x, M_y, and M_z are each component of $\boldsymbol{M}$, and $\boldsymbol{B}$ is the applied magnetic field, including B_0 and B_1. M_0 is equilibrium net magnetization right after polarization. The new parameter T_1 is the time constant that explains the recovery of longitudinal magnetization, and it is also called as spin−lattice relaxation time. And T_2 is the time constant that explains the decay of transverse magnetization, and another name is spin−spin relaxation time. Typically T_2 is smaller than T_1.

We can assume that the B_0 field points the z−axis. With this assumption, the above equation can be divided into each component as follows.

$$\frac{dM_x}{dt} = \gamma\left(M_y B_0\right) - \frac{M_x}{T_2}$$
$$\frac{dM_y}{dt} = \gamma(-M_x B_0) - \frac{M_y}{T_2}$$
$$\frac{dM_z}{dt} = \frac{M_0 - M_z}{T_1}$$

If we introduce another parameter $M_{xy} = M_x + iM_y$, the first two equations are further simplified to

$$\frac{dM_{xy}}{dt} = -i\gamma B_0 M_{xy} - \frac{M_{xy}}{T_2}$$

Finally, if we denote γB_0, which is Larmor frequency, as ω_0, the final equation for M_{xy} and M_z is derived as

$$M_z(t) = M_0\left(1 - \exp\frac{t}{T_1}\right)$$
$$M_{xy}(t) = M_{xy}(0)\, exp\left(-\frac{t}{T_2}\right) exp\left(-i(\omega_0 t + \phi)\right)$$

Figure 1.3 shows an example plot of M_{xy} and M_z. Initially, the magnetization was pointing x−axis, which means it has been excited. We can see that the magnetization recovers to the z−axis, while the transverse magnetization precesses in Larmor frequency, which

perfectly describes the phenomenon in NMR.

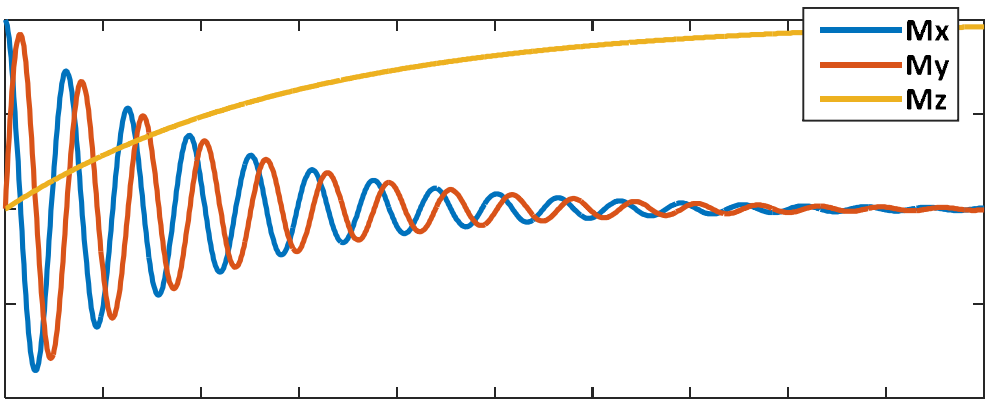

Figure 1.3 An example plot of $\boldsymbol{M_{xy}}$ and $\boldsymbol{M_z}$. We can clearly see that as time goes on, the magnetization recovers to z−axis, and transverse magnetization precesses in Larmor frequency.

1.1.4 Image Formation

In NMR spectroscopy, which uses the NMR to investigate the properties of organic molecules by exploiting the fact that atomic nuclei has certain magnetic property, receives the net signal coming from every molecule that has been excited. This signal lacks the spatial information, therefore making an image out of it impossible. As a result, additional localization should be added to make an image. This spatial encoding is achieved by adding a field called the gradient field. This gradient field is spatially linear magnetic field in the direction of B_0 field. The spatial variation is given in all x, y, and z direction, and each component is called G_x, G_y, and G_z. As these gradient fields modify the magnitude of B_0, it results in different resonance frequency, which means each location produces a signal with various frequency. This relation can be explained by

Fourier transform.

To explain this further, let us consider the case where G_x was applied after excitation. Since gradient fields are spatially linear, the following equation can express G_x.

$$G_x(x,t) = G_x(t)x\hat{z}$$

With this field, the equation for transverse magnetization $\mathbf{M_{xy}}$ is now modified to

$$M_{xy}(x,t) = M_{xy}(x,0)\,exp\left(-\frac{t}{T_2}\right)exp\left(-i\left(\omega_0 t + \gamma\left(\int G_x(t)dt\right)x + \phi\right)\right)$$

If we demodulate the received signal by ω_0, ignore the initial phase ϕ, and neglect T_2 term, we have the equation

$$M_{xy}(x,t) = M_{xy}(x,0)\,exp\left(-i\gamma\left(\int G_x(t)dt\right)x\right)$$

Since the received signal is proportional to the sum of the above component from all coordinate, we need to integrate the above by x. If we further modify this to a more familiar term by introducing $k_x = \frac{\gamma}{2\pi}\int G_x(t)dt$,

$$S(k_x) \propto \int M_{xy}(x,0)\,exp(-i2\pi k_x x)\,dx$$

This equation is identical to Fourier transform. Therefore, inverse

Fourier transform can reconstruct the received signal $S(k_x)$ to $M_{xy}(x,0)$. The same process can be applied to all three axes. Therefore it is possible to get the 3D image. The domain formed by x, y, and z is called the image domain, and domain created by k_x, k_y, and k_z is called K-space domain.

It is important to note that the coordinate of the signal in K-space is determined by the time integral of the gradient field. In other words, changing the gradient field can modify the strategy to collect K-space data. The timing, magnitude, and order of the applied gradient field and B_1 field, or RF pulse, is called pulse sequence.

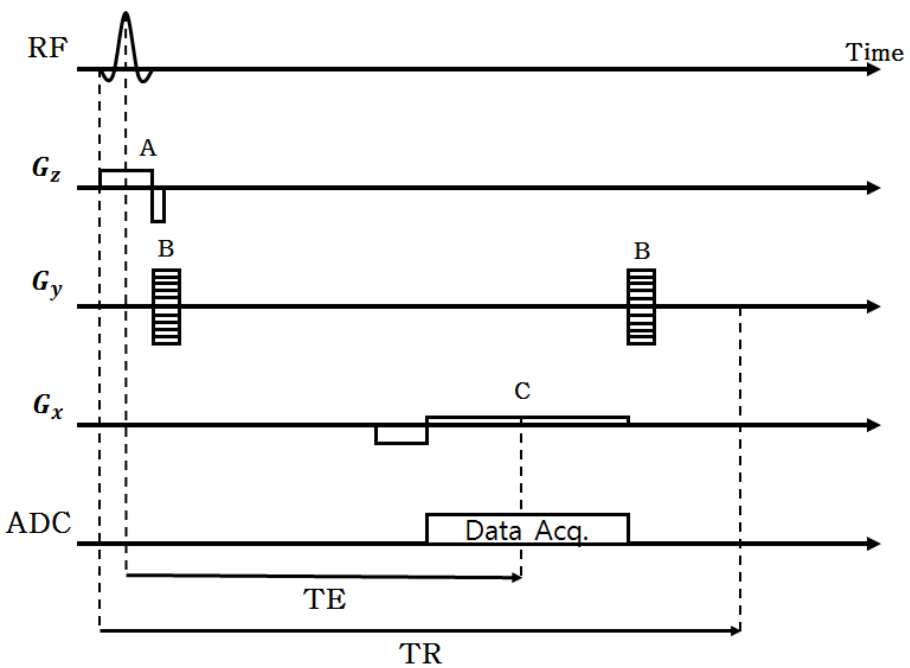

Figure 1.4 A pulse sequence diagram for two-dimensional gradient echo imaging. The pulse sequence includes the information about the timing and magnitude of how the gradient fields and RF pulse should be applied. Each gradient has specific functions: A is slice selection gradient, B is phase encoding gradient, and C is frequency

encoding gradient.

Figure 1.4 illustrates a basic pulse sequence diagram for two-dimensional gradient echo imaging. RF stands for the RF pulse used to excite the magnetization, and G_x, G_y, and G_z are the three orthogonal gradient fields. In Figure 1.4, A is the slice selection gradient, which enables selective excitation in one axis when combined with RF pulse. B and C are the spatial encoding gradient which was previously explained. In practice, B is called the phase encoding gradient, and C is referred to as the frequency encoding gradient. A single run of the above pulse sequence produces a single line of K-space data of a single slice. When it is repeated multiple times, the desired full K-space data can be acquired. The duration of each repetition is called the repetition time, or TR, and the time between the center of excitation to the center of data acquisition is called the echo time or TE. Figure 1.5 shows the acquisition trajectory by the pulse sequence in Figure 1.4.

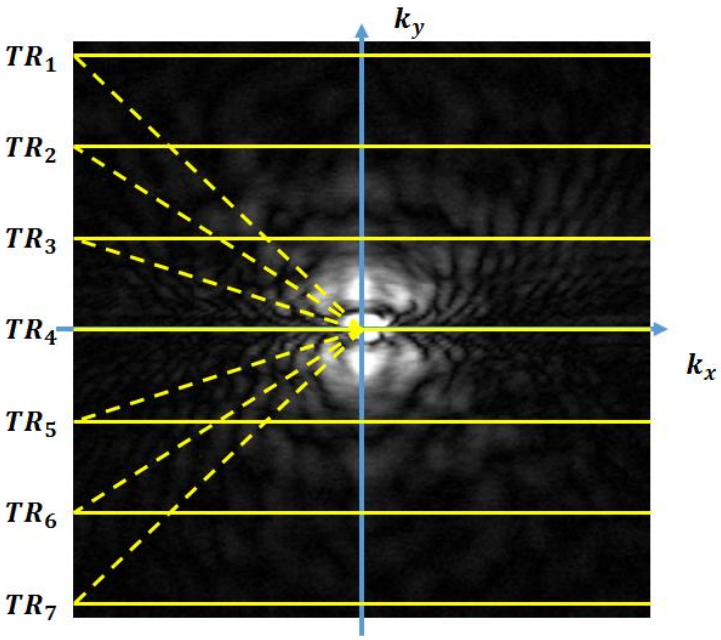

Figure 1.5 The data acquisition trajectory in K-space. A single repetition acquires a single line in K-space. The order of phase encoding gradients and their number determines the order and number of acquired lines.

The significance of MRI come from the fact that by modifying the pulse sequence and applying post-processing, various image contrasts can be achieved as shown in Figure 1.6. This flexibility is one of the differentiating features of MRI which allowed its use in different fields and applications. Even though many pulse sequences have been developed, novel contrast mechanisms remain to be discovered by MR engineers.

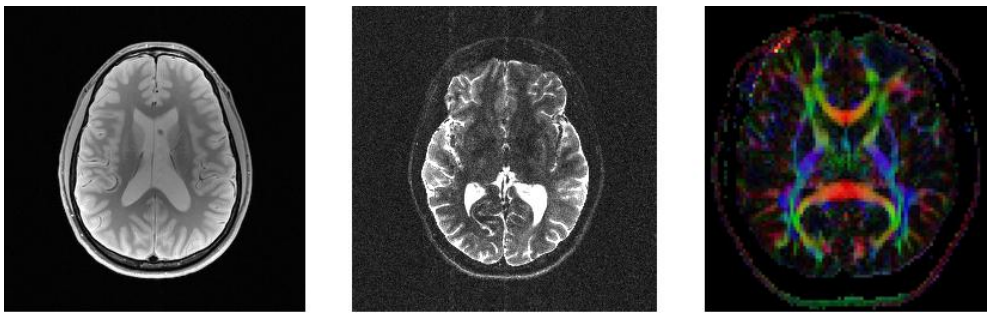

Figure 1.6 Example of different contrast images in MRI.

1.2 Spin Echo Imaging

The spin echo imaging is one of the most commonly used imaging mechanism in both clinics and research. Also, the main research of this dissertation targets on accelerating the image acquisition of spin echo imaging. The background theory of spin echo imaging and conventional acceleration schemes will be introduced.

1.2.1 Theory

The spin echo was first described by Hahn in 1950 [5]. The fundamental concept of spin echo is the use of the refocusing RF pulse. The refocusing RF pulse is an RF pulse with 180 degrees flip angle. The effect of this additional RF pulse is that it refocuses phase dispersion of magnetization caused by local field inhomogeneity.

To explain this further, Figure 1.7 illustrates the concept. As shown in Figure 1.7.a, all magnetization produced by nuclei in the imaging volume are aligned to a single direction right after

excitation. However, if the imaging volume contains local field homogeneities generated by magnetic susceptibility effect or chemical shift, each magnetization precess in various frequencies according to the magnetic field. This results in dispersion of individual magnetization as shown in Figure 1.7.b. If a signal is retrieved at this time point, the sum of magnetization vectors is smaller than the sum of absolute values of magnetization vectors, which means signal loss. Such situation is critical in gradient echo imaging, where signal nulls in regions with large field inhomogeneity. The application of refocusing pulse solves this problem. The comparison between gradient echo imaging and spin echo imaging is shown in Figure 1.8.

When the refocusing pulse is applied, the phase of all magnetizations is negated. Figure 1.7.c shows this. Since the direction of phase accumulation is preserved after the refocusing pulse, the negated phase accumulation of individual magnetization diminishes to zero when the equal time from excitation to refocusing has passed after refocusing. As a result, we can get the maximum signal output shown in Figure 1.7.d. The data acquired at this time point is called the spin echo.

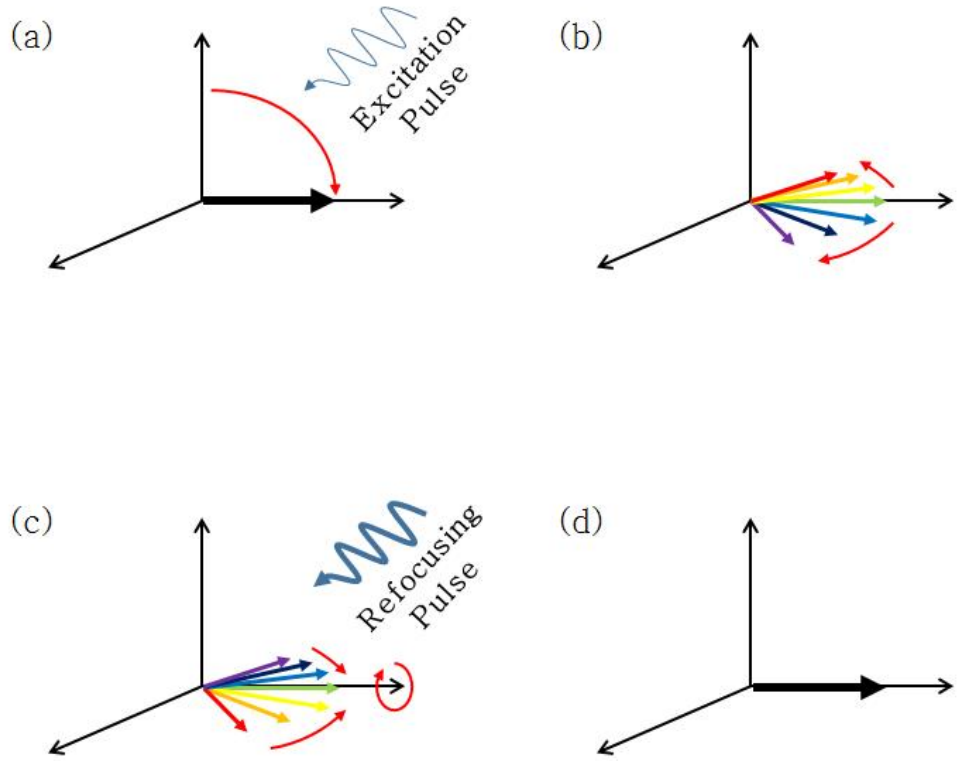

Figure 1.7 The process of formation of the spin echo. **a.** After the excitation pulse is applied, the magnetizations of individual nuclei point the same direction, achieving maximum net magnetization. **b.** If the imaging nuclei contain field inhomogeneity, dispersion of individual magnetization occurs by different resonance frequency. **c.** When a refocusing pulse is applied, the sign of the accumulated phase is reversed. Since the direction of phase accumulation is preserved, the dispersed magnetizations get refocused. **d.** At the time point where the same time from excitation to refocusing has passed after refocusing, spin echo is formed.

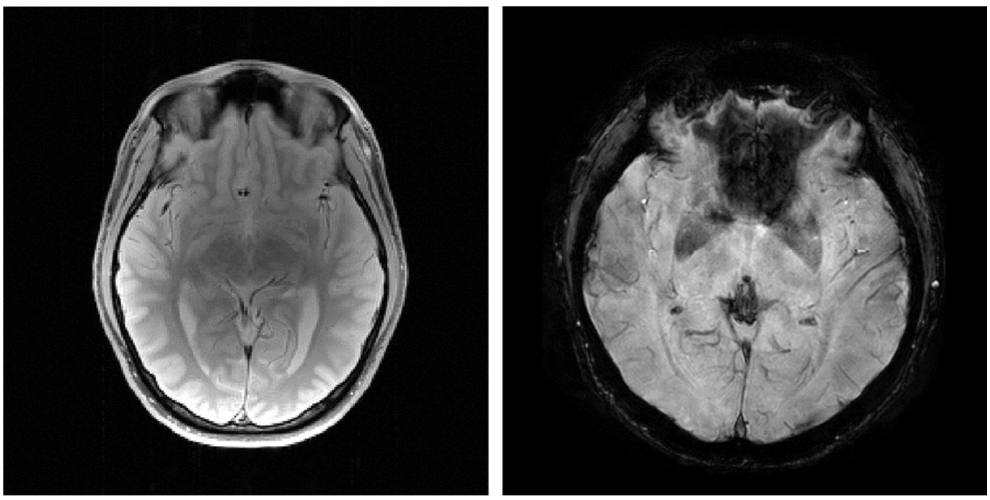

Figure 1.8 The comparison image of spin echo imaging (left) and the gradient echo imaging (right). In the area with large inhomogeneity, spin echo imaging preserves the image, whereas gradient echo imaging the signal is almost nulled.

1.2.2 Pulse Sequence Diagram

Figure 1.9 shows the pulse sequence diagram of a typical spin echo imaging. The pulse sequence diagram is analogous to the pulse sequence diagram of two-dimensional gradient echo imaging in Figure 1.4. Additionally, the acquisition trajectory in K-space of Figure 1.9 is equivalent to Figure 1.5. The difference is the refocusing RF pulse added between the excitation and the data acquisition. Since the refocusing RF pulse should be placed in the middle between the excitation and the data acquisition, the time between the excitation pulse and refocusing pulse and between the refocusing pulse and data acquisition is half the TE.

One drawback of spin echo imaging compared to gradient echo imaging is the inevitable increase of minimum TE. Also, to achieve desired contrast and signal-to-noise ratio (SNR), TR of spin echo

imaging is in the order of hundreds of milliseconds to several seconds. Compared to tens to hundreds of milliseconds order of TR in gradient echo imaging, the scan time of spin echo imaging is usually very long. As a consequence, acceleration methods such as partial Fourier reconstruction and gradient and spin echo (GRASE) imaging is needed.

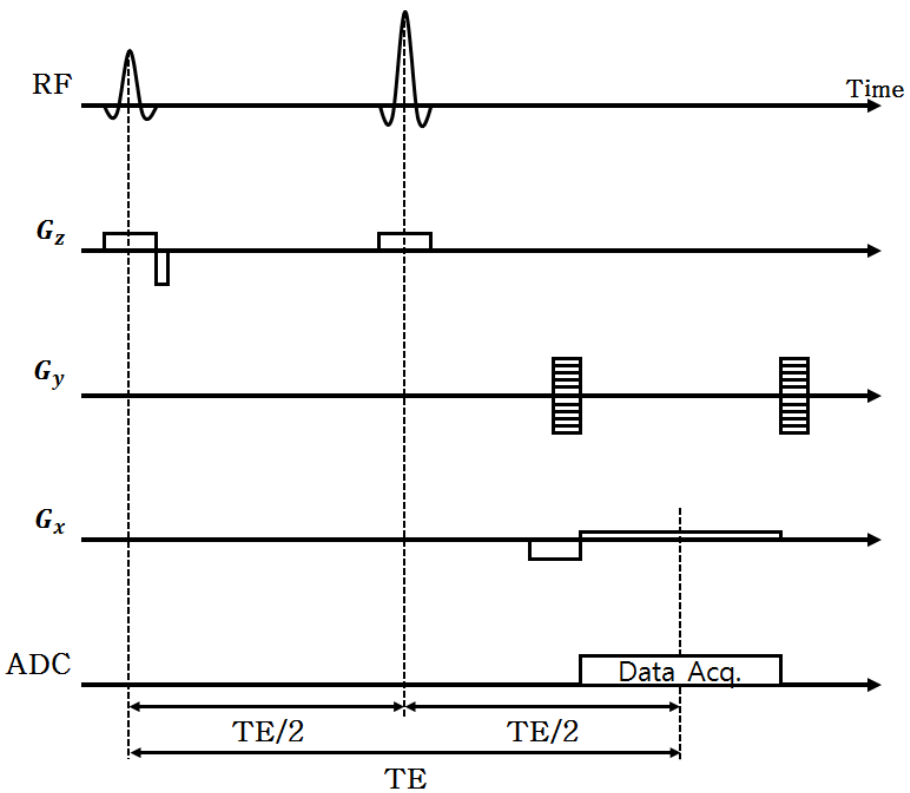

Figure 1.9 The pulse sequence diagram of spin echo imaging. The refocusing RF pulse is located right in the middle between the center of data acquisition and excitation. Through this strategy, the image suffers less from field inhomogeneity artifacts.

1.2.3 Partial Fourier Reconstruction

When a real signal is Fourier transformed, the result follows a condition called conjugate symmetry [6]. It means that the conjugate of a data point is equal to the data point where their positions are symmetric according to the origin. As a result, if we can assume that the original data is real, we can construct the data with only half of the full Fourier transformed data. Since smaller data is collected, a shorter scan time can be achieved.

However, this assumption is not valid in MRI practice. If we consider a receiver coil, magnetizations in different locations need to travel different paths, especially in the distance, which results in the different phase of collected signals. The different phase is well shown in Figure 1.10.

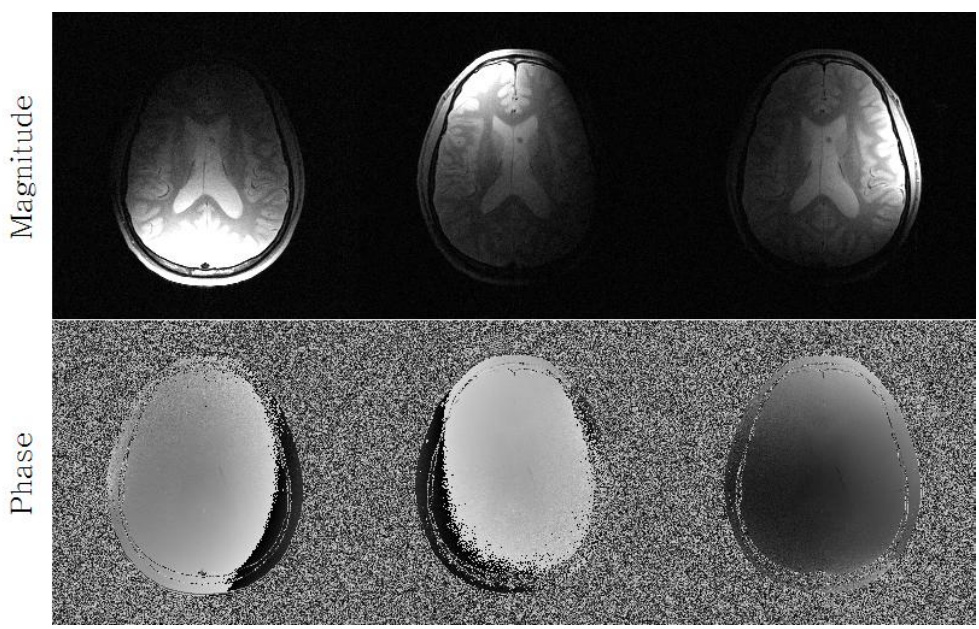

Figure 1.10 Magnitude and phase map of an MRI image collected by different receivers. Due to coil geometry, the phase map varies by the distance between the receiver and certain location in image.

Since the assumption that the original image is real cannot be achieved, we cannot use conjugate symmetry condition directly. However, as we can see from Figure 1.10, the phase of the collected image is smooth in nature. Using this knowledge, we can assume that a low-resolution phase map is enough to estimate the original phase of the image. With this assumption, we can apply conjugate symmetry to fill up missing data portion where its symmetric pair is collected. This technique is called partial Fourier reconstruction.

The procedure is illustrated in Figure 1.11. If the data is collected more than 50 %, the symmetric data strip in the center can be used to construct a low-resolution phase map. Then the image is divided by this low-resolution phase map. Because the initial assumption was that the low-resolution phase map is a good estimate of the true phase of the image, the result of previous division can be assumed as real, enabling the use of conjugate symmetry condition to fill out the missing data portion. Since the major assumption was that the low-resolution phase map is identical to original phase map, reconstruction errors are located in regions with sharp phase change such as vessels and fat. Also, if the acquisition portion decreases, the low-resolution phase map becomes more inaccurate, resulting in increased reconstruction error.

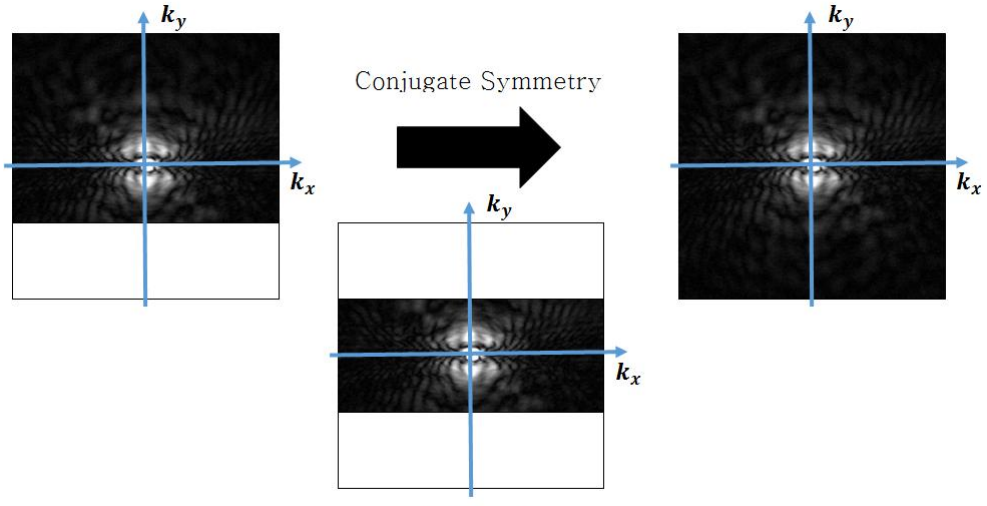

Figure 1.11 The partial Fourier reconstruction algorithm using conjugate symmetry. The symmetric center data from collected partial data is Fourier transformed to construct a low-resolution phase map. Using the low-resolution phase map, the missing data portion is filled by conjugate symmetry condition.

1.2.4 Gradient and Spin Echo Imaging (GRASE)

For conventional spin echo imaging, single line is collected after a refocusing pulse. To accelerate the acquisition, gradient and spin echo or GRASE pulse sequences [7, 8] use a train of alternating polarity readout gradients to acquire multiple lines after a refocusing pulse. If these lines are encoded differently, the total scan is accelerated by the number of readout gradients. Normally three gradient echoes are collected.

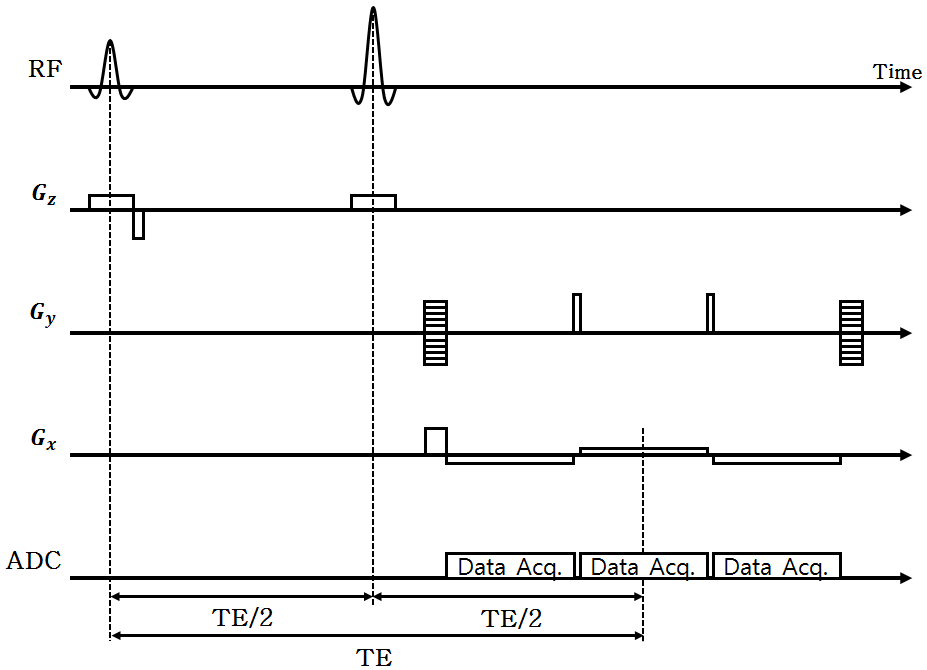

Figure 1.12 The pulse sequence diagram of GRASE imaging. The phase encoding gradients between the data acquisitions enable each readout to fill different lines in K-space. The total acceleration achieved by this sequence is factor of 3.

Figure 1.12 displays the GRASE pulse sequence which acquires three lines after an RF pulse. Since the middle portion of K-space has the most information, the readout placed in spin echo time is used to fill the middle portion. Figure 1.13 shows an example of K-space encoding.

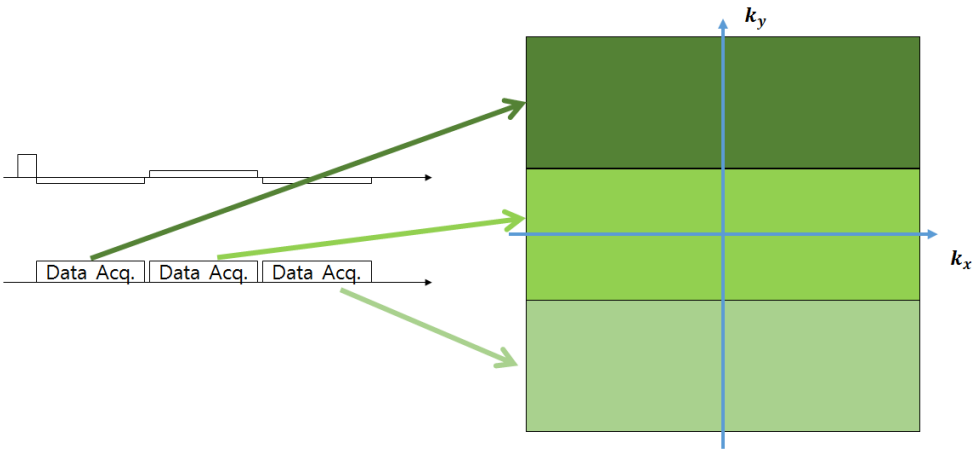

Figure 1.13 An example of K-space encoding by GRASE. Each readout fills evenly distributed portion of K-space.

One drawback of GRASE imaging comes from the discontinuity in K-space produced by different echoes. The time difference between the echoes leads to difference in both phase and magnitude of the signal. Such inconsistency produces ringing artifacts at regions with large field inhomogeneity and $T2^*$ decay as shown in Figure 1.14.

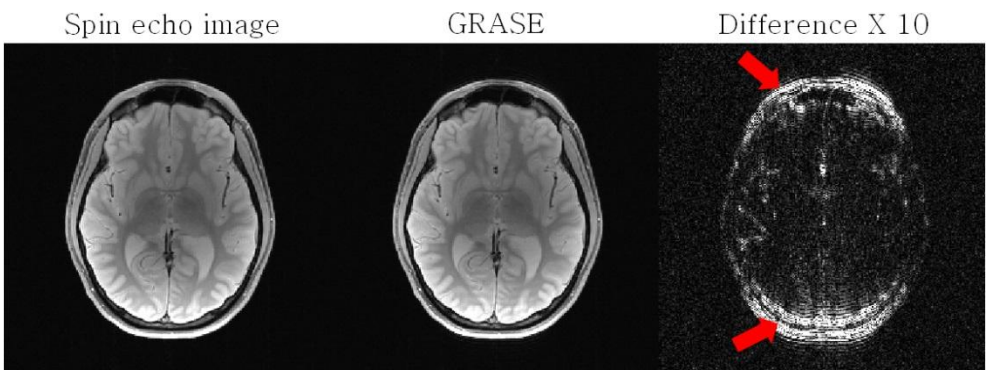

Figure 1.14 A comparison of spin echo imaging and GRASE imaging. Since the middle part of K-space is filled with the spin echo, the overall contrast does not change. However, the regions with large $T2^*$ decay or large field inhomogeneity generates ringing artifact, indicated by red arrows.

Chapter 2. Dual Echo Trajectory

2.1 Introduction

Spin echo imaging, due to its robustness to field inhomogeneity and chemical shifts, is one of the most commonly used imaging method in the clinic. To accelerate the data acquisition, several methods such as partial Fourier acquisition [9], Fast Spin Echo (FSE) [10, 11], Gradient Echo And Spin Echo (GRASE) [7, 8], parallel imaging [12, 13], compressed sensing [14] have been proposed.

Among them, the GRASE method acquires multiple echoes (typically three echoes) per excitation and, therefore, accelerates the total scan time by the number of echoes gained for each refocusing pulse. However, the centers of three readouts are separated by the length of a readout. This produces notable phase difference as well as signal decay between the echoes acquired at different timing. Therefore GRASE images suffer from artifacts near regions with fast $T2^*$ decay or large field inhomogeneity.

Still, acquiring multiple echoes to accelerate imaging is still an attractive approach. To alleviate the problems the GRASE imaging has, the proposed method, Dual Echo Trajectory (DuET), acquires two partial echoes immediately before and after the spin echo time to accelerate data acquisition. With this approach, the collected two echoes have smaller time difference then GRASE imaging, therefore reducing the artifact in GRASE imaging. Moreover, since the echoes

are very close to spin echo, the resulting image has a similar contrast to spin echo image, including its robustness to local field inhomogeneity. Also, echo timing correction was used to reduce the artifact. To reconstruct the missing portion of the partial echoes, iterative partial Fourier reconstruction method called projection onto convex sets (POCS) algorithm was used [15]. The proposed method was evaluated on phantom and in vivo experiments. Also, the proposed method was compared with conventional spin echo imaging with partial Fourier acquisition.

2.2 Methods

2.2.1 Pulse Sequence Diagram

Figure 2.1.a shows the pulse sequence diagram of the proposed method. The conventional spin echo imaging collects data at spin echo time, and the time point is marked by A. In GRASE imaging, multiple full echoes were obtained including the spin echo. In the proposed method, two partial echoes are collected instead of one full echo. The two echoes are placed symmetrically on the spin echo time A, and the direction of the partial acquisition was chosen in opposite direction so the echo centers of the two echoes are closer to each other and the spin echo time. The timing B in Figure 2.1.a indicates the echo centers of the partial echoes. The time spacing between the echo center and the spin echo time is denoted as the gap time in this study.

Figure 2.1.b shows K-space encoding scheme of the proposed method. The blue echo, the former echo, and the yellow echo, the latter echo, fills up half of phase encoding each. The former echo fills up the middle portion of K-space, and since the right part of echo is omitted, missing data portion is located at the right side of K-space. The latter echo fills up the edges of K-space, and the opposite data portion is missing compared to the blue echo.

The reason for filling the middle portion of K-space with former echoes is its resemblance to original spin echo. Since both partial echoes have time gap to spin echo time, they include signal decay

due to intravoxel dephasing. The difference between former echo and latter echo is that the former echo experiences less T2 decay than both spin echo and the latter echo, considering the time duration after excitation pulse. Therefore for the former echo, the two effects cancels each other, leading to less contrast difference compared to conventional spin echo.

Another reason for choosing this K-space coverage was because the missing K-space should be reconstructed by partial Fourier reconstruction. The required condition for partial Fourier reconstruction to work is that for the missing data point that to be recovered, its origin-symmetric data point should be attained. The used acquisition scheme satisfies this condition, allowing the use of partial Fourier reconstruction.

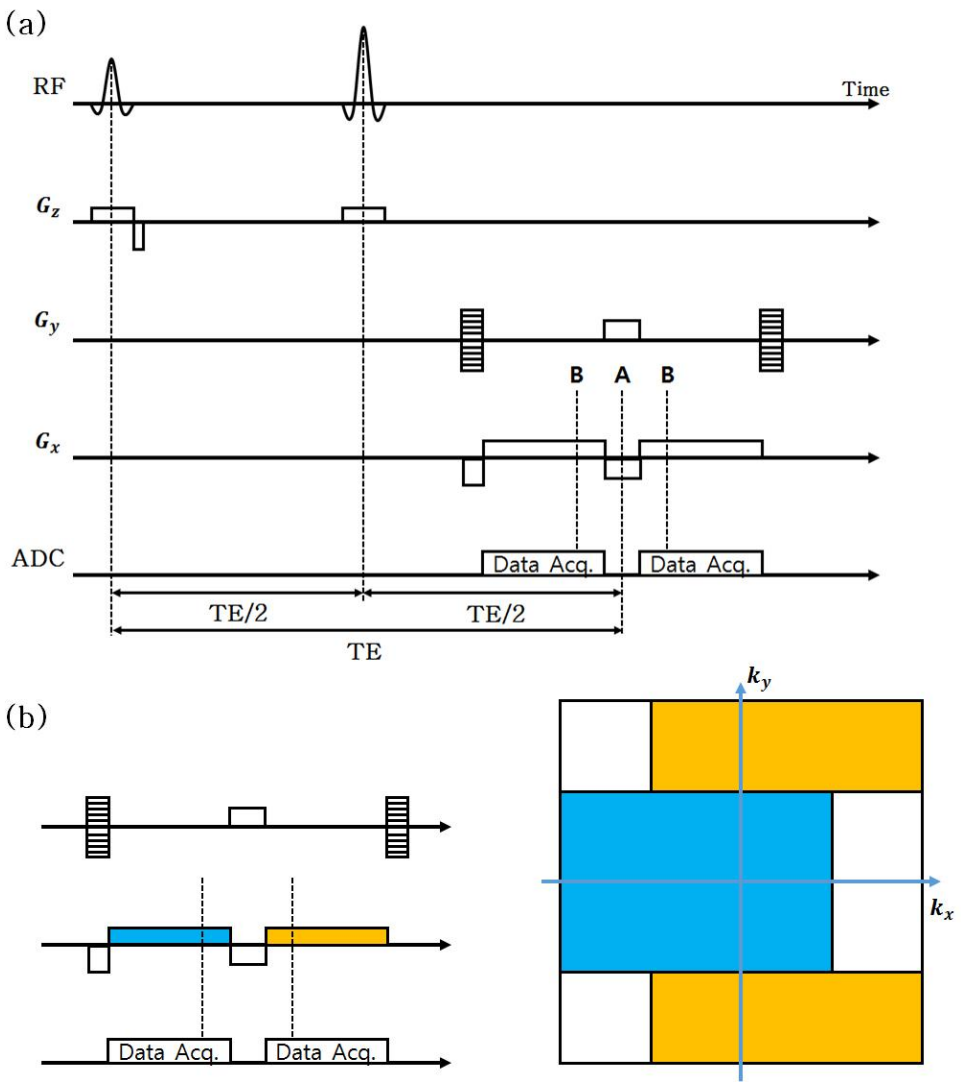

Figure 2.1 The **(a)** pulse sequence diagram and **(b)** K-space coverage map. **(a)** Two partial echoes are placed symmetrically on the spin echo time **A**. The centers of partial echoes are denoted as **B**. Through this scheme, the two collected echoes are very close to spin echo, therefore preserving the image contrast and its robustness to field inhomogeneity. **(b)** The K-space is filled by both former and latter echo. This method allows partial Fourier reconstruction to fill the missing part while minimizing the discontinuity in K-space made by different echoes.

2.2.2 Echo Timing Correction

The pulse sequence diagram in Figure 2.1.a shows the gradient lobe used to rewind and phase encode between the partial echoes should be as short as possible to minimize the gap time. To make the gradient lobe as short as possible, the gradient lobe should use the maximum gradient amplitude and slew rate. In practice, the use of maximum amplitude and slew rate often leads to an inaccurate gradient amount. Such erroneous gradient amount leads to discrepancy in K-space center of each partial echo, in other words, echo timing. In current K-space acquisition, such difference leads to high-frequency artifact since the boundary between the two echoes exists in that frequency range.

To account for the difference in echo timing, an EPI-like echo timing correction was implemented. To calibrate the difference, an additional readout was acquired without phase encoding at the first TR. Since this dummy TR was originally inserted for the signal to reach a steady-state, there is no increase in the acquisition time. Using the knowledge that shift in K-space results in linear phase in the image domain, we can derive the echo timing discrepancy by comparing the acquired echoes. The procedure is shown in Figure 2.2. The echo timing is corrected before reconstruction.

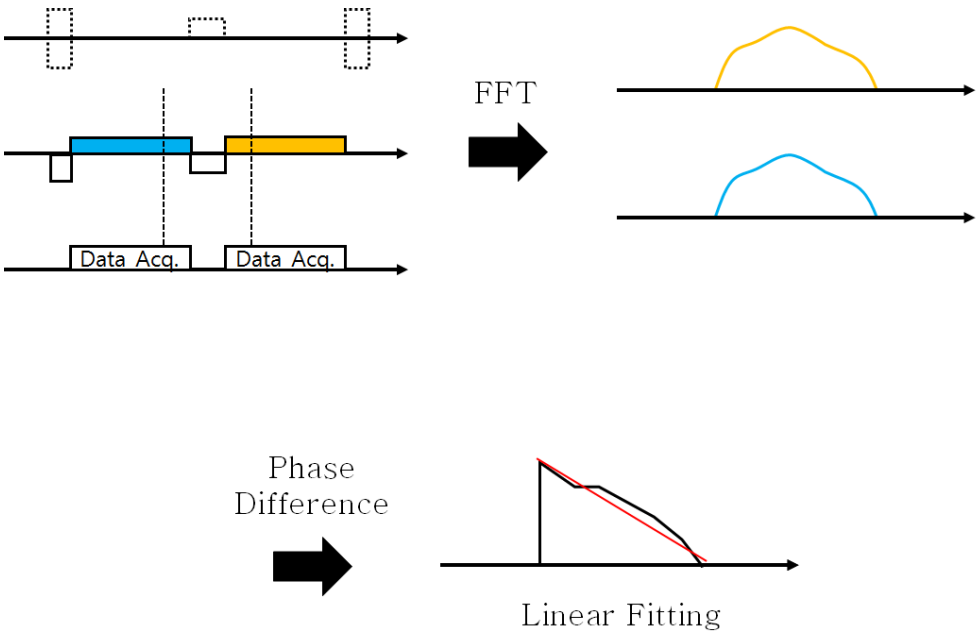

Figure 2.2 The procedure of calibrating echo timing error. An additional acquisition without any phase encoding acquires the center line of K-space for each readout. Since the shift in one domain is Fourier transformed to linear phase, the two data are Fourier transformed, and their phase difference is linearly fitted to estimate the shift in the echo timing.

2.2.3. Projection Onto Convex Sets (POCS)

After the correction, the projection onto convex sets (POCS) [15] algorithm reconstructs the missing parts of the K-space. POCS algorithm is an iterative algorithm that constructs the K-space by constantly applying two steps. In the first step, the originally collected data replaces the K-space data consistently during the iteration. And in the second step, the low-resolution phase map replaces the phase map in the image space during the iteration. Figure 2.3 illustrates the algorithm.

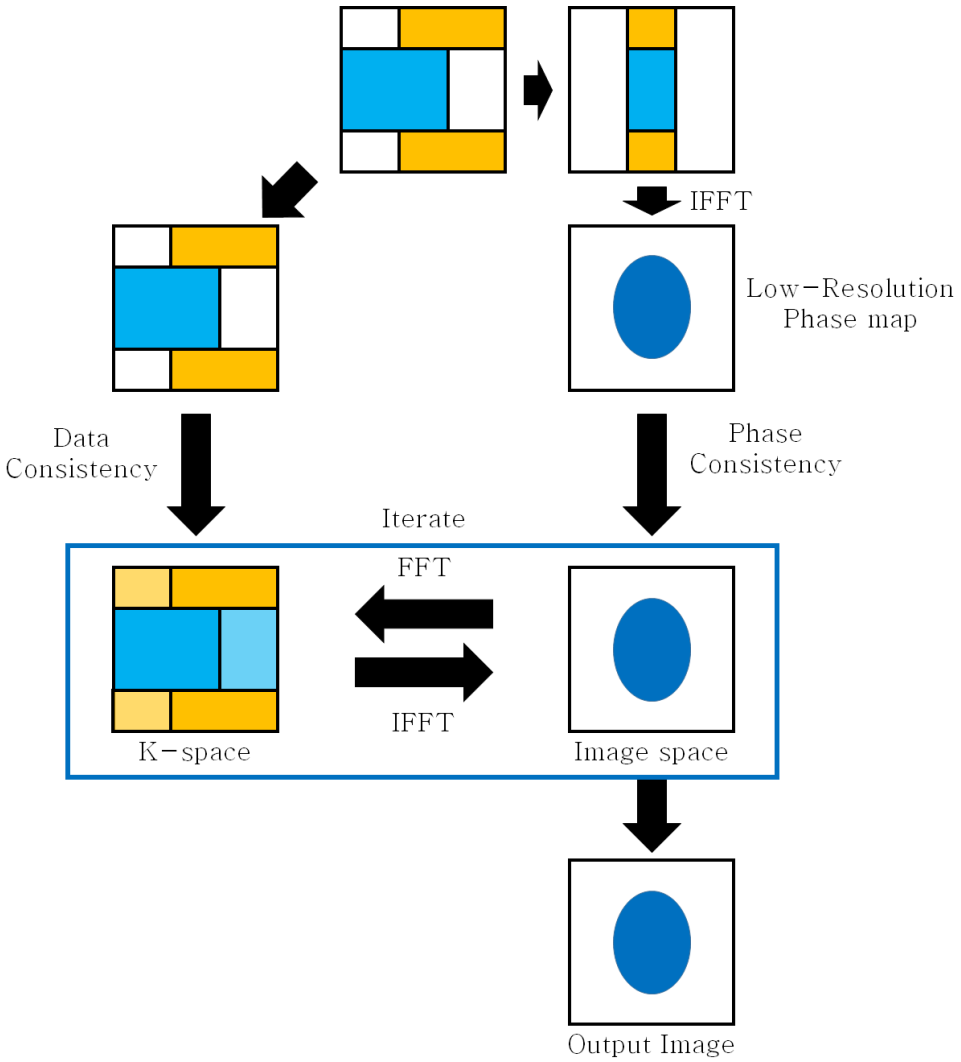

Figure 2.3 The POCS algorithm used to reconstruct the image. The center symmetric data strip in the collected data is used to generate the low-resolution phase map. During the iteration, in K-space the attained data replaces the data being reconstructed, and the low-resolution phase map replaces the phase of the image. After 5 iterations, the iteration ends.

2.2.4. Parameter Optimization

In the proposed method, the important parameter to choose is the gap time or equivalently the size of the symmetric center strip. In the echo consistency point of view, smaller gap time leads to less signal decay and phase accumulation, which results in reduced artifact made by K-space discontinuity. However, to reduce the gap time, the acquisition ratio of the partial echo should decrease. In partial Fourier reconstruction, cutting the acquisition ratio causes the low-resolution phase map to become more inaccurate compared to the true phase map. As a result, there is a tradeoff between the artifact generated by data inconsistency and the reconstruction error.

For choosing the optimal gap time and partial acquisition ratio, in vivo scans were conducted with a range of gap time and partial acquisition ratio. The chosen range of acquisition ratio was from 62.5 % to 87.5 %. Other parameters are as follows : single slice, FOV = 256×256 mm2, resolution = 1×1 mm2, slice thickness = 5 mm, and TR/TE = 650/12 ms. The normalized root means squared error (nRMSE) to the conventional spin echo image was used as the comparison criterion. The following equation was used to calculate the nRMSE.

$$nRMSE = \sqrt{\frac{\sum(I - I_{ref})^2}{\sum I_{ref}^2}}$$

The following is the meaning of the notations. I : target image, I_{ref} : reference image (conventional spin echo).

2.2.5. Phantom Study

With the optimized parameters, a phantom was imaged using the spin echo imaging and the proposed method. The scan parameters were as follows: single slice, FOV = 256×256 mm2, resolution = 1×1 mm2, slice thickness = 5 mm, and TR/TE = 650/12 ms. For the proposed method, gap time Δt = 0.78 ms, and center strip width = 128 samples. An off-resonance saturation pulse was applied to saturate fat signal. The acquisition time was 2.77 min for the conventional spin echo and 1.39 min for the proposed method.

2.2.6. In Vivo Study

In vivo scans on single healthy volunteer were conducted to evaluate the efficiency of the proposed method. Two scans of the conventional spin echo imaging and a scan of the proposed method was conducted. The second scan of conventional spin echo imaging was used to generate partial Fourier acquisition images with different acquisition ratio ranging from 52 % to 75 %. The generated images were compared with the proposed method considering nRMSE, using the first spin echo image as the reference. The scan parameters are identical to the phantom study except for the number of slices. In in vivo scan, 16 slices were scanned using the interleaved multislice technique. To assess the effect of the interleaved multislice technique, additional single slice images were obtained.

2.3 Results

2.3.1 Parameter Optimization

Figure 2.4 shows the result of scan while varying the gap time. The sampled gap times are 520, 640, 780, 900, and 1040 us. The corresponding partial acquisition ratios are 62.5 %, 68.75 %, 75 %, 81.25 %, and 87.5 %. The nRMSE plot shows that the optimal gap time was 780 us, which is 75 % in acquisition ratio. The 128 center strip width and gap time 0.78 ms used in phantom and in vivo study was used according to this result.

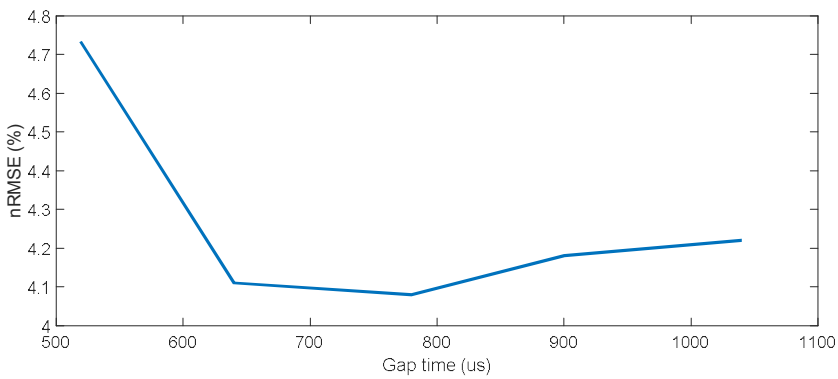

Figure 2.4 The nRMSE plot according to the gap time. The x-axis denotes the gap time, and the y-axis indicates the calculated nRMSE. Due to the tradeoff between the data inconsistency artifact and the reconstruction error, the optimal gap time was 780 us, or 75 % in acquisition ratio.

As expected, the tradeoff between the data consistency and the data reconstruction was apparent in the nRMSE plot. The image

also showed the tradeoff. Figure 2.5 shows the resulting images. To show the tradeoff, region with artifacts from data inconsistency is indicated by the red box denoted as A in Figure 2.5.a. Also, the blue box B in Figure 2.5.a shows the region with artifact from reconstruction. Figure 2.5.b and 2.5.c are the magnified images of each box A and B. Figure 2.5.b shows the increase of ringing artifact indicated by yellow arrows as the gap time increases. On the other hand, Figure 2.5.c shows the decrease of reconstruction error as the gap time increases, also indicated by yellow arrows. It is evident that the gap time 780 us shows moderate error in both regions.

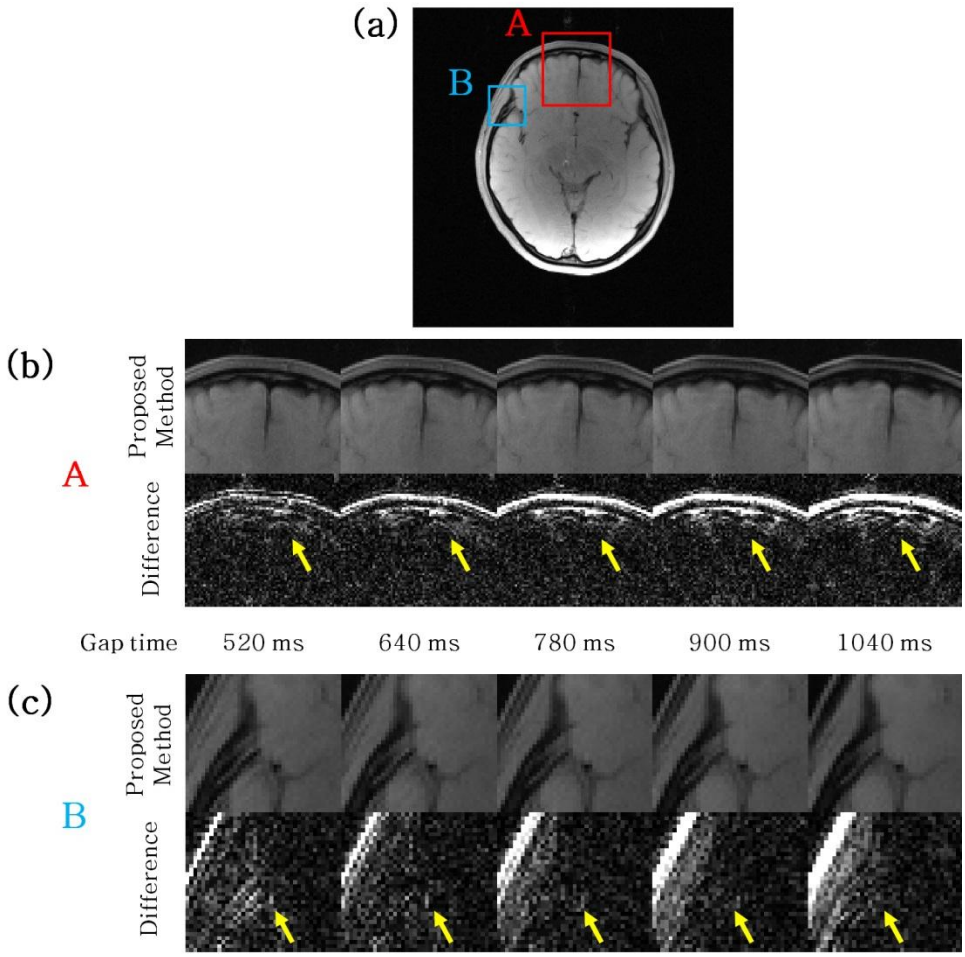

Figure 2.5 The comparison images of the proposed method with different gap time. **(a)** The red box A indicates the region with data inconsistency artifact, and the blue box B indicates the region with reconstruction error. **(b)** Magnified image of box A of the proposed method and difference map to the reference spin echo image. Since increased gap time leads to increased data inconsistency, the ringing artifact increases. **(c)** Magnified image of box B of the proposed method and difference map to the reference spin echo image. Since increased gap time leads to more accurate reconstruction, the reconstruction error decreases.

2.3.2 Phantom Study

Figure 2.6 shows the result of the phantom scan. The difference map shows that the proposed method produces a similar image to the conventional spin echo as expected. The only notable error is located on the edges. The POCS algorithm used in reconstruction explains this since it is known to produce reconstruction error in sharp phase changes. However, the overall nRMSE is small (nRMSE = 1.33 %).

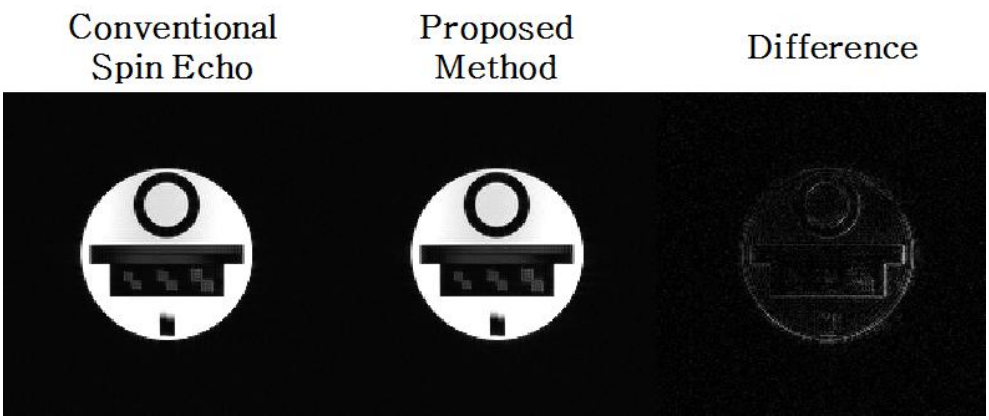

Figure 2.6 The comparison of conventional spin echo imaging and the proposed method. The difference map is magnified by 10. The overall image is almost identical with 1.33 % nRMSE.

2.3.3 In Vivo Study

Figure 2.7 shows the result of the in vivo scan. In Figure 2.7.a The difference is significant only in non-brain regions with fast $T2^*$ decay. Other brain regions show only noise-like difference map. Also, comparing the difference map and the field inhomogeneity map in Figure 2.7.b, there is no distinct resemblance. The nRMSE of the brain region was 4.28 %. This means that the proposed method produces an image similar to the conventional spin echo imaging, both in image contrast and in robustness to local field inhomogeneity.

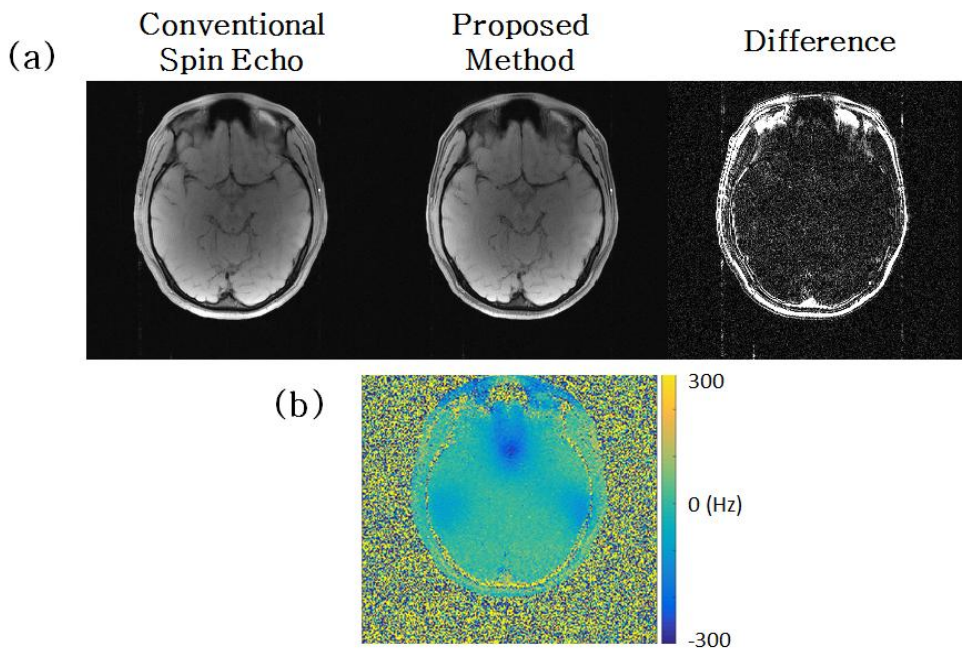

Figure 2.7 (a) The comparison between the conventional spin echo imaging and the proposed method. The difference map was multiplied by 10. The proposed method does not display any contrast difference in brain region other than noise-like difference.

(b) The field inhomogeneity map of the imaged slice. Even though extreme field inhomogeneity with maximum 250 Hz was applied, the proposed method does not generate any significant error.

Figure 2.8 shows the nRMSE plot of the proposed method and generated conventional partial Fourier acquisition imaging. The crossing point was made when the partial acquisition ratio was 60 %. According to this result, the proposed method takes 16.7 % less acquisition time than the conventional partial acquisition with the same nRMSE. This implies that the proposed method some advantages over the conventional partial acquisition.

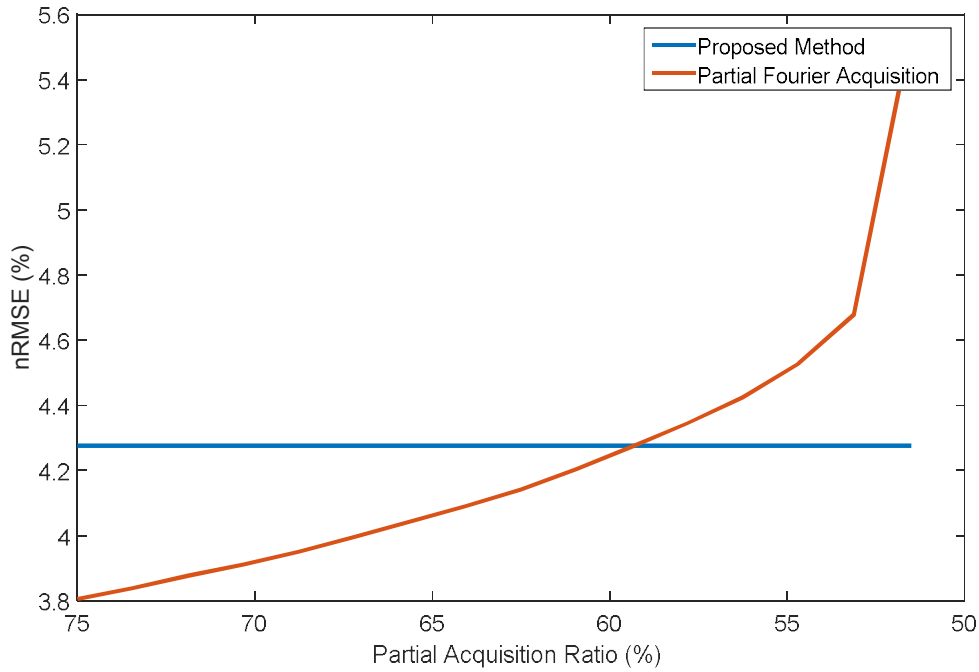

Figure 2.8 The nRMSE plot of DuET and generated partial Fourier acquisition image. x-axis denotes partial Fourier acquisition ratio used to generate the corresponding image, and y-axis shows the

nRMSE. The crossing point was made when partial acquisition ratio was 60 %.

Figure 2.9 shows the comparison between the single slice scan and interleaved multislice scan of the proposed method. The ringing artifact indicated by red arrows was significantly reduced with the application of interleaved multislice technique. The reason behind this was the saturation of the flow signal. With interleaved multislice, the flowing blood gets constantly excited and dephased during the acquisition, and this results in decreased flow signal. The partial Fourier reconstruction used in the proposed method produces such ringing artifact because the low-resolution phase map often fails to correctly estimate the true phase in regions like vessels since they are small in size.

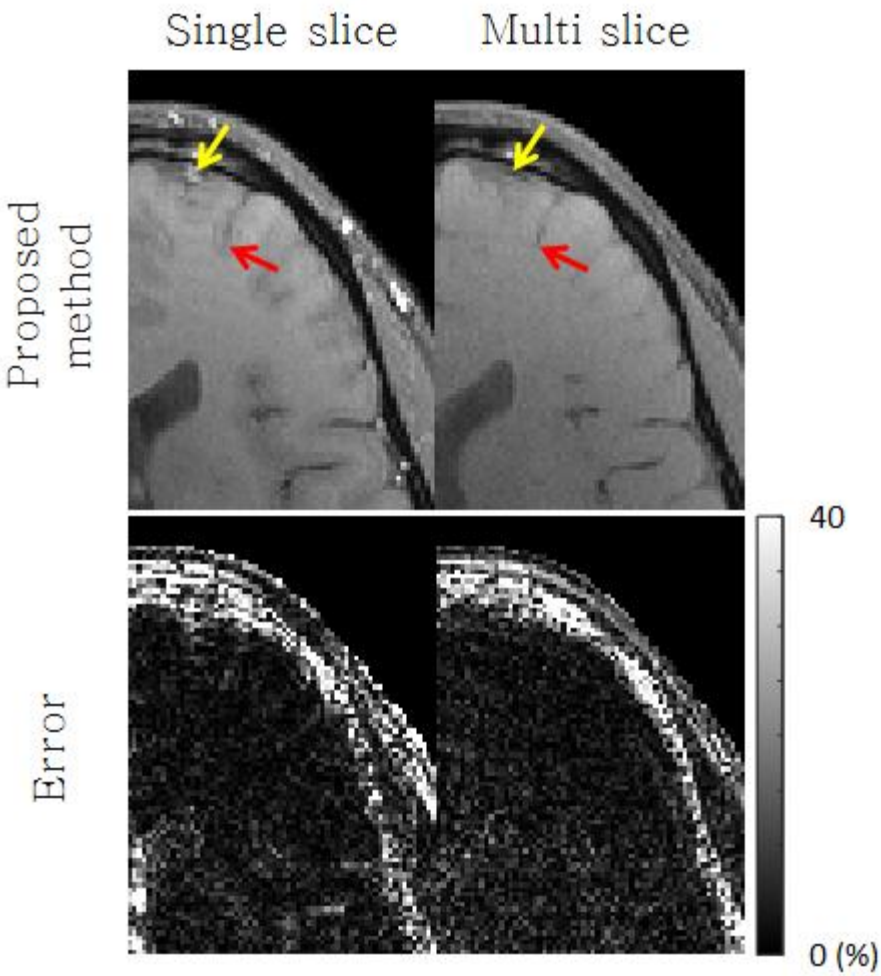

Figure 2.9 The comparison between single slice and interleaved multislice scan. The red arrows indicate the ringing artifact, which decreased with interleaved multislice. This was caused by decreased vessel signal indicated by yellow arrows.

2.4 Discussion and Conclusion

In this study, the proposed method, Dual Echo Trajectory, was implemented and compared to conventional spin echo imaging and partial Fourier acquisition. The original intention to preserve the image contrast and robustness to field inhomogeneity of original spin echo imaging was achieved. The phantom and in vivo study validated this, showing low nRMSE (1.33 % for phantom, 4.28 % for in vivo) compared to spin echo imaging. Also the comparison to partial Fourier acquisition and even showed that the proposed method has some advantages over it. It is also important to note that this method is compatible with other acceleration methods such as SENSE and GRAPPA.

The present study has several limitations. First of all, the performance can be varied with acquiring matrix size. For this study, 256 by 256 matrix data was acquired. If 512 by 512 matrix data is to be obtained, fixing the gap time allows 62.5 % partial acquisition, which was considered inadequate in the result. Therefore, additional optimization should be conducted for different acquisition matrix size. Also, without the fat saturation pulse, the proposed method suffers severe artifact. The data inconsistency artifact is large in fat because it has both large chemical shift and signal magnitude. Further study on how to handle this artifact source should be considered.

In conclusion, the proposed Dual Echo Trajectory pulse sequence successfully accelerates the scan time of spin echo imaging by two

without harming the image contrast nor introducing additional artifact due to field inhomogeneity.

References

1. Nishimura, D.G., *Principles of magnetic resonance imaging*. 1996: Stanford University.
2. Bernstein, M.A., K.F. King, and X.J. Zhou, *Handbook of MRI pulse sequences*. 2004: Elsevier.
3. Purcell, E.M., H. Torrey, and R.V. Pound, *Resonance absorption by nuclear magnetic moments in a solid.* Physical review, 1946. **69**(1-2): p. 37.
4. Bloch, F., *Nuclear induction.* Physical review, 1946. **70**(7-8): p. 460.
5. Hahn, E.L., *Spin echoes.* Physical review, 1950. **80**(4): p. 580.
6. Bracewell, R., *The fourier transform and iis applications.* New York, 1965. **5**.
7. Oshio, K. and D.A. Feinberg, *GRASE (Gradient-and Spin-Echo) imaging: A novel fast MRI technique.* Magnetic resonance in medicine, 1991. **20**(2): p. 344-349.
8. Feinberg, D.A. and K. Oshio, *GRASE (gradient-and spin-echo) MR imaging: a new fast clinical imaging technique.* Radiology, 1991. **181**(2): p. 597-602.
9. McGibney, G., et al., *Quantitative evaluation of several partial Fourier reconstruction algorithms used in MRI.* Magnetic resonance in medicine, 1993. **30**(1): p. 51-59.
10. Hennig, J., *Multiecho imaging sequences with low refocusing flip angles.* Journal of Magnetic Resonance (1969), 1988.

78(3): p. 397-407.

11. Hennig, J., A. Nauerth, and H. Friedburg, *RARE imaging: a fast imaging method for clinical MR.* Magnetic resonance in medicine, 1986. **3**(6): p. 823-833.
12. Pruessmann, K.P., et al., *SENSE: sensitivity encoding for fast MRI.* Magnetic resonance in medicine, 1999. **42**(5): p. 952-962.
13. Griswold, M.A., et al., *Generalized autocalibrating partially parallel acquisitions (GRAPPA).* Magnetic resonance in medicine, 2002. **47**(6): p. 1202-1210.
14. Lustig, M., D. Donoho, and J.M. Pauly, *Sparse MRI: The application of compressed sensing for rapid MR imaging.* Magnetic resonance in medicine, 2007. **58**(6): p. 1182-1195.
15. Haacke, E., E. Lindskogj, and W. Lin, *A fast, iterative, partial-Fourier technique capable of local phase recovery.* Journal of Magnetic Resonance (1969), 1991. **92**(1): p. 126-145.

국문초록

자기공명영상법의 발명으로 인체에 해로운 방사선 피폭에 의한 위험이 없이 뇌의 영상을 얻을 수 있게 되었다. 자기공명영상의 도움으로 많은 연구자는 뇌의 비밀에 대한 의문점들을 해결해 나가고 있다. 자기공명영상의 가장 큰 장점은 다양한 방법으로 서로 다른 특성을 갖는 영상들을 얻는 것으로, 특히 스핀에코 영상기법의 경우 T1, T2 강조영상 등과 같은 중요한 정보를 갖고 있는 영상을 자장불균질성에 의한 영상 손실이 없이 얻어낼 수 있다. 본 논문에서는 이 스핀에코 영상을 더 빠르게 얻을 수 있는 새로운 방법을 제시하였다. 이 방법에서는 새로운 펄스열을 개발하였다. 원래 스핀에코 하나를 얻는 방법에서 스핀에코 주위로 두 개의 부분에코를 얻어서 영상획득 속도를 2배로 향상시키고, 얻지 않은 부분을 부분 푸리에 재구성연산을 통해 얻게 된다. 위 방법을 통하여 자기공명영상을 영상 손실을 최소화하며 가속화할 수 있다.

주요어 : 자기공명영상법, 스핀에코영상법, 고속영상시퀀스

학 번 : 2015-20908